Sensors & Actuators: A. Physical 397 (2026) 117300

Contents lists available at ScienceDirect

Sensors and Actuators: A. Physical

journal homepage: www.journals.elsevier.com/sensors-and-actuators-a-physical

Experimental-based Cramér-Rao lower bound estimation of triaxial accelerometer calibration methods using Monte Carlo simulation

Dariusz Maton [a,*], John T. Economou [a], David Galvão Wall [a], Irfan Khan [a], Robert Cooper [a], Simon Trythall [b], Stuart Kitching [b]

[a] Centre for Defence Engineering and Physical Sciences, Cranfield University, Defence Academy of the United Kingdom, Shrivenham, Swindon SN6 8LA, United Kingdom
[b] BAE Systems, Rochester, Kent ME1 2XX, United Kingdom

ARTICLE INFO

Keywords:
Accelerometer
Calibration
Triaxial
MEMS
Monte Carlo
Inertial

ABSTRACT

Low-cost accelerometers can be found in many systems requiring accurate attitude estimation. Their unique thermomechanical responses necessitate frequent recalibrations to maintain a certain level of performance. Established accelerometer calibrations are the six position and multi-position methods requiring static conditions. This paper presents a Monte Carlo simulation comparing these for a sensor with a comprehensive set of calibration errors in the model. Precision of the simulations are compared with the Cramér-Rao lower bound (CRLB) and, for the first time, the CRLB for the six-position method is defined. For the multi-position method, calibration accuracy of six algorithms is assessed by Monte Carlo simulation. The precision of the best performing algorithm is compared with the CRLB using experimental data. The effect of parameter initialisation on the algorithms is observed via simulation and experimentally with two algorithms shown to have sensitivity to initialisation. The types and order of positions sampled in the multi-position method are analysed for the case when only the minimum number are available. Cardinal positions are shown to be best in terms of calibration accuracy and precision.

1. Introduction

Inertial sensors such as accelerometers and rate gyroscopes are autonomous sensors capable of operating independent of any supporting infrastructure in the environment [1]. Inertial measurement units (IMUs) are typically packages of triaxial gyros and accelerometers sensing angular velocities and specific forces of the sensor reference frame relative to the inertial respectively. With advances in micro-electromechanical systems (MEMS) manufacturing, low-cost, lightweight, and efficient IMUs are used in many electronic systems requiring attitude estimation such as smartphones, human-machine interfaces and autonomous vehicles [2,3]. This requires fusion of angular rates from the gyros and gravimetric attitude inferred by the accelerometers. As the former contain biases that drift with time and temperature, the latter are relied upon for periodic attitude corrections under static conditions [4].

Accelerometers also exhibit drift however. For low-cost proof mass MEMS accelerometers, the unique stresses induced during first level packaging (FLP) are decisive in defining its performance and stability [5]. Considering how hysteresis complicates attempts at model-based compensation, frequent recalibration of accelerometers becomes more attractive [6]. Established methods of accelerometer calibration are static methods and include the six position (SPM) and multi-position method (MPM).

1.1. Triaxial sensor model

The general linear model of the triaxial sensor relates the vector of measurements, $\mathbf{v} = \begin{bmatrix} v_x & v_y & v_z \end{bmatrix}^{\mathrm{T}}$, to the inputs (accelerations), $\mathbf{a} = \begin{bmatrix} a_x & a_y & a_z \end{bmatrix}^{\mathrm{T}}$, by:

$$\mathbf{v} = \mathbf{STMa} + \mathbf{b} \tag{1}$$

Where $\mathbf{b} = \begin{bmatrix} b_x & b_y & b_z \end{bmatrix}^{\mathrm{T}}$ is a vector of biases, $\mathbf{S}$ is a diagonal matrix of scale factors (SFs) for each axis:

* Corresponding author.
E-mail addresses: d.maton@cranfield.ac.uk (D. Maton), j.t.economou@cranfield.ac.uk (J.T. Economou), d.galvaowall@cranfield.ac.uk (D.G. Wall), irfan.khan2@cranfield.ac.uk (I. Khan), r.a.cooper@cranfield.ac.uk (R. Cooper), simon.trythall@baesystems.com (S. Trythall), stuart.kitching@baesystems.com (S. Kitching).

https://doi.org/10.1016/j.sna.2025.117300
Received 19 July 2025; Received in revised form 31 October 2025; Accepted 16 November 2025
Available online 17 November 2025
0924-4247/© 2025 The Authors. Published by Elsevier B.V. This is an open access article under the CC BY license (http://creativecommons.org/licenses/by/4.0/).

$$\mathbf{S} = \begin{bmatrix} s_x & 0 & 0 \\ 0 & s_y & 0 \\ 0 & 0 & s_z \end{bmatrix} \tag{2}$$

The orientation of three nonorthogonal sensor axes with respect to the orthogonal platform axes can be described by six angles [7]. Arbitrarily choosing the sensor x-axis as the reference for nonorthogonality (the sensitivity of one axis to excitation in another), these angles can be decomposed into three orthogonalisation (α, β, γ) and misalignment angles (ϕ, θ, ψ) which are captured in the **T** and **M** matrices respectively [8]. For small α, β, γ, **T** is:

$$\mathbf{T} = \begin{bmatrix} 1 & 0 & 0 \\ -\alpha & 1 & 0 \\ \beta & -\gamma & 1 \end{bmatrix} \tag{3}$$

The assumption of an arbitrary reference axis is necessary for unique α, β, γ and gives **T** its lower triangular structure [9]. Nonorthogonalities arise due to defects in the sensor caused during manufacture or by design such as when proof masses are shared between axes.

The misalignment matrix, **M**, describes the misalignment of the orthogonalised sensor axes relative to orthogonal platform axes. These can occur during FLP resulting in misalignments of less than 1° [5]. Assuming xyz rotation order, **M** is defined as:

$$\mathbf{M} = \begin{bmatrix} c(\theta)c(\psi) & -c(\theta)s(\psi) & s(\theta) \\ c(\phi)s(\psi) + s(\phi)s(\theta)c(\psi) & c(\phi)c(\psi) - s(\phi)s(\theta)s(\psi) & -s(\phi)c(\theta) \\ s(\phi)s(\psi) - c(\phi)s(\theta)c(\psi) & s(\phi)c(\psi) + c(\phi)s(\theta)s(\psi) & c(\phi)c(\theta) \end{bmatrix} \tag{4}$$

The product of **STM** is described in this work as the matrix of axis sensitivities which capture the combined effects of SFs, nonorthogonalities and misalignments:

$$\mathbf{STM} = \begin{bmatrix} k_{xx} & k_{xy} & k_{xz} \\ k_{yx} & k_{yy} & k_{yz} \\ k_{zx} & k_{zy} & k_{zz} \end{bmatrix} \tag{5}$$

This results in a linear model with 12 calibration parameters (CPs). Nonlinearity for accelerometers tends to be a small fraction of a percent of the full-scale range (FSR) and is thus safely ignored [8].

1.2. The six-position method (SPM)

SPM has been described in other works as the six-point, turnover and minmax method. It involves the sequential rotations of the triaxial accelerometer by exact 180° rotations of levelled platform axes such that each sensor axis gets exposed to antiparallel effects of gravity [10]. Implementations often involve mounting the sensor triad inside a perfect cube or two-axis rotary table which can achieve accurate rotations.

Forming two matrices containing these measurement vectors:

$$\mathbf{V}_{g+} = \begin{bmatrix} \mathbf{v}_{x,g+} & \mathbf{v}_{y,g+} & \mathbf{v}_{z,g+} \end{bmatrix} \tag{6}$$

$$\mathbf{V}_{g-} = \begin{bmatrix} \mathbf{v}_{x,g-} & \mathbf{v}_{y,g-} & \mathbf{v}_{z,g-} \end{bmatrix} \tag{7}$$

Averaging antiparallel measurements reveals biases along the main diagonal:

$$\mathbf{b} = \mathrm{diag}\left(1/2\left(\mathbf{V}_{g+} + \mathbf{V}_{g-}\right)\right) \tag{8}$$

In Ferraris et al. [10], SFs were estimated from the square root of elements on the main diagonal of the right-hand side of Eq. (9). Note **M** has disappeared from the right-hand side having unit norm, $\mathbf{M}\mathbf{M}^{\mathrm{T}} = \mathbf{I}$:

$$\frac{1}{4g^2}\left(\mathbf{V}_{g+} - \mathbf{V}_{g-}\right)\left(\mathbf{V}_{g+} - \mathbf{V}_{g-}\right)^{\mathrm{T}} = \mathbf{S}\mathbf{T}(\mathbf{S}\mathbf{T})^{\mathrm{T}} \tag{9}$$

In their work, the misalignment matrix was estimated as Eq. (10) which ignored the contribution from the nonorthogonality matrix, **T**:

$$\mathbf{M} = \frac{1}{2g}\mathbf{S}^{-1}\left(\mathbf{V}_{g+} - \mathbf{V}_{g-}\right) \tag{10}$$

It has been suggested nonorthogonalities are not recoverable in the SPM with specialist equipment being required to estimate them [10–12]. Conversely, others have proposed a version of the SPM incorporating the triangular matrix **T** and ignoring **M** in the calibration [13]. In the most comprehensive approaches, the SPM has been proposed with matrix decompositions to recover both nonorthogonality and misalignment matrices [9,14]. Using the Cholesky decomposition to effectively take the square root of the left side of Eq. (9) and obtain the triangular matrix, **R**:

$$\mathbf{R} = chol\left(\frac{1}{4g^2}\left(\mathbf{V}_{g+} - \mathbf{V}_{g-}\right)\left(\mathbf{V}_{g+} - \mathbf{V}_{g-}\right)^{\mathrm{T}}\right) \tag{11}$$

The LU decomposition then extracts **S** and **T**. **M** can then be calculated by:

$$\mathbf{M} = \frac{1}{2g}(\mathbf{S}\mathbf{T})^{-1}\left(\mathbf{V}_{g+} - \mathbf{V}_{g-}\right) \tag{12}$$

The conflicting views on the ability to distinguish between misalignment and nonorthogonality via the SPM are interesting. Ultimately, the validity of this method depends on the validity of the model assumed in Eq. (1) – Eq. (4). Whether or not this is representative of the real sensor or a convenience that enables more elements in **STM** to be captured is unknown. Indeed, some have used symmetric axis sensitivity matrices, explaining it is more suitable for MEMS accelerometers as it captures cross coupling effects between axes [15]. Considering the noise and resolution limitations of real low-cost accelerometers, trying to distinguish misalignment and nonorthogonality may not even be practical. For this reason, it may be useful to derive the variance defined by the Cramér-Rao lower bound (CRLB) as in [8], which gives a more realistic representation of the achievable precision of calibration.

1.3. The multi-position method (MPM)

The multi-position (or multipoint) calibration method uses accelerometer measurements of the reaction force due to gravity for multiple orientations to return optimal CPs [16]. For a triaxial sensor, it is effectively a 3D ellipsoid fitting problem [17]. A well-calibrated sensor should give measurement vectors whose magnitudes equal gravity for any arbitrary orientation under static conditions [11]. Many have reported variations, using different algorithms to minimise the cost function in Eq. (13) [15,17–20]:

$$J = \underset{s_x,s_y,s_z,\alpha,\beta,\gamma\in\mathbb{R},\mathbf{b}\in\mathbb{R}^3}{\mathrm{argmin}} \sqrt{\frac{1}{n}\sum_{i=1}^{n}\left[\,|\mathbf{g}| - \left|\mathbf{T}^{-1}\mathbf{S}^{-1}(\mathbf{v}-\mathbf{b})\right|\,\right]^2} \tag{13}$$

Glueck et al. and Ye et al. introduced online methods but, as they still require sampling a sequence of positions, it is not clear if much advantage is offered over offline methods [21,22].

It has been suggested that convergence of Eq. (13) is not always reliable with influencing factors including the number and types of positions sampled, the number of unknowns in the model as well as the parameters used for initialisation [11,19]. These observations suggest nonconvexity in the MPM.

For initialisation, using values bounded by the datasheet has been advised [19]. While closed form methods avoided the problem of parameter initialisation altogether [23], the parameters used far exceeded reasonable bounds thus, failure of the iterative methods to reach the correct parameters may not have been representative of their actual performances. In earlier works, the reported biases were large compared to what can be expected from low-cost MEMS accelerometers these days and this has been noted in later works with improvements in MEMS manufacturing techniques [11,21]. Hence, it is possible the convergence of the MPM to the correct solution is no longer affected by

parameter initialisation as suggested.

In terms of the positions themselves, sampling first the cardinal positions before arbitrary ones has been recommended [11]. The results of Tee et al. supported this, with singular solutions occurring when any of the three axes were underrepresented in the procedure [13].

Various algorithms have been used to minimise Eq. (13) including least-squares adjustment [11], Gauss-Newton (G-N) optimisation [15], Levenberg–Marquardt (L-M) algorithm [12], and quasi-Newton (Q-N) optimisation [18]. While little difference between Q-N and L-M algorithms was shown in [12], their method may have been flawed as their calibration metric was based on the difference between the magnitude of accelerometer measurements and gravity. This is understandable as it is not possible to know the true CPs but may be problematic because, given the possible nonconvexity, a minimised cost function may not guarantee accurate calibration. A better way of assessing algorithm performance would be by Monte Carlo simulation of the sensor and calibration procedure, for which the true CPs are known. This would give a more representative view of the calibration accuracy achieved by different algorithms. This approach was taken in [8,21], but inter-algorithm performance was not investigated.

Although a minimum of nine are required in the MPM, sampling more than 24 equally spaced positions was recommended in [18]. The effect of number of positions on calibration has been well studied with results supporting use of a number in the mid-20s [12,15]. In the simulations of [21], hundreds of positions were sampled which may not be practical.

Compared with the SPM, the MPM frees the requirement for perfect 180° rotations of the sensor and related equipment. It returns estimates of SF, nonorthogonality and bias parameters (nine in total). Misalignment angles between sensor and platform axes cannot be estimated in the MPM as **M** is assumed an orthonormal matrix which is eliminated in the calculation of the magnitude of the measurements in Eq. (13) [14]. Thus, some works have presented additional steps to detect and correct residual misalignments. This involves minimising the sinusoidal dispersion generated when fully rotating the platform about one of the attitude axes [14,17,24]. This reintroduces the need for perfect rotations about the platform axes however, negating the main advantage of the MPM.

This paper presents for the first time a Monte Carlo simulation of SPM and MPM calibrations to assess their accuracies. Contrary to experimental work, modelling the accelerometer gives knowledge of the true CPs and thus, the ability to report accuracies. To best represent the real sensor, the model is made to contain a comprehensive set of errors. Details of these are presented in the Methods in 2. Results in 3 compare the precision of the simulated MPM with experimental data from four low-cost triaxial accelerometers and its CRLB. For the first time, the CRLB is also derived for the SPM and compared with the simulations. Inter-algorithm accuracy for the MPM is reported with additional simulations confirming an optimum sequence of positions when only nine are available. Simulation and experimental results study the effect of initialisation on the MPM with two algorithms shown to be sensitive to initialisation on the experimental data. 4 discusses the results in detail with key findings summarised in the Conclusion in 5.

2. Methods

2.1. Monte Carlo simulation

For simulating the calibration methods, a low-cost triaxial accelerometer was modelled according to Eq. (1) – Eq. (4) using MATLAB's *imusensor* system object. Characteristics of a low-cost accelerometer from the LSM6DS3TR-C IMU were used: FSR of 2 g, resolution 0.06 mg/LSB, maximum biases of ±40 mg, maximum scale factor error ±3 % of FSR, maximum nonorthogonality and misalignment angles of ±1°, noise density 400 μg/$\sqrt{\text{Hz}}$, rate random walk 2 μg$\sqrt{\text{Hz}}$ and bias instability 0.04 mg. Misalignment and nonorthogonality angles were not given in the datasheet so were inferred based on values in literature [5,9]. Both misalignment and nonorthogonality were added for greater realism. Noise error properties were inferred from an Allan variance noise analysis with 13-hour data set sampling a real LSM6DS3TR-C at 100 Hz. The effective bandwidth of the simulated sensor was 50 Hz which matched the configuration of the real IMUs with their antialiasing and high pass filters disabled.

To simulate the SPM and MPM, purely kinematic rotational trajectories were generated. Combined with the accelerometer model, simulated measurements were made as shown in Fig. 1. For the MPM, a nominal value of 26 equidistant positions were used to avoid singular solutions. These were identical to those in [11]. Data points for each position were taken in the steady state condition, averaging 100 samples to reduce the impact of noise as also done in [8]. The dynamics of the calibration platform were not modelled. A real implementation would require additional steps to ensure only steady state conditions are sampled which may increase the calibration duration

For representative results, a Monte Carlo approach was used. Results were generated for 200 calibration scenarios with randomised accelerometer model whose calibration errors were sampled from a normal distribution with 3σs represented by the bounds of each error. 200 scenarios were chosen as, after 100 simulations, the average CE changed less than 1 % of the previous value so it was doubled and used.

To compare calibration methods, SPMs replicated from literature were those of Ferraris et al. [10], Jurman et al. [14], and Tee et al. [13]. MPMs were Rohac et al. [18], Sipos et al. [12], Frosio et al. [15], Syed et al. [11], Merayo's method [25], and minimum volume enclosing ellipsoid (MVEE) [26]. For the methods of Rohac et al. and Sipos et al., quasi-Newton and L-M methods were implemented using MATLAB's *fminunc* and *lsqnonlin* functions respectively. The L-S adjustment of Syed et al. was implemented to the best of the author's ability using details from [27,28]. The method of Frosio et al. was replicated based on code by [29]. It was noted for Frosio et al. that a symmetric matrix for axis sensitivities was originally used which did not agree with the model in the other works. It was therefore modified to ensure a fair comparison with the other algorithms. For the MPMs, initialisation parameters for the optimisation algorithms were also sampled from a uniform distribution of their minimum and maximum values. For fair inter-algorithm comparison on the MPM, each had a maximum of 400 iterations, function tolerance of 1e-6 and the same cost function.

To observe the choice of positions in the MPM on calibration accuracy, four scenarios were simulated assuming only nine positions could be sampled: random positions, six cardinal positions followed by three random, six rotated cardinal positions followed by three random and three random positions followed by six cardinal. The last case was of interest to see if the order of positions mattered. The rows in Fig. 2 show the four scenarios. Again, a Monte Carlo simulation with 200 iterations was performed.

2.2. Calibration error (CE) metric

In works using experimental data, the magnitude of accelerometer measurements relative to gravity have been used to measure calibration accuracy [12]. As mentioned, simulation allows knowledge of true CPs lending to a more reliable metric for assessing algorithm performance. Like in [21], a relative metric, the mean calibration error ($\overline{CE}$), was defined as in Eq. (14):

$$\overline{CE} = \frac{k_{calib}}{N}\sum_{n=1}^{N}\left[\frac{1}{9}\sum_{i=1}^{3}\sum_{j=1}^{3}\frac{\left|k_{ij,true}-k_{ij,est}\right|}{k_{ij,norm}}\right] + \frac{1-k_{calib}}{3}\sum_{n=1}^{N}\left[\sum_{k=1}^{3}\left(\frac{b_{i,true}-b_{i,est}}{b_{i,norm}}\right)\right] \tag{14}$$

Where k_{calib} is a weight adjusted depending on the relative importance of SFs and biases. A value of 0.3 was used to put greater weight on bias

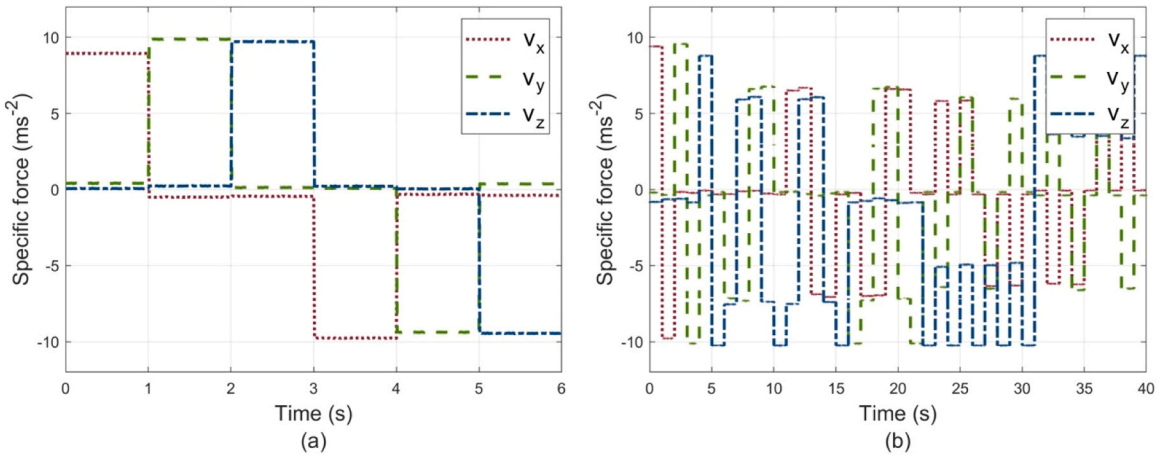


Fig. 1. Simulated accelerometer measurements for (a) SPM and (b) MPM (26 positions).

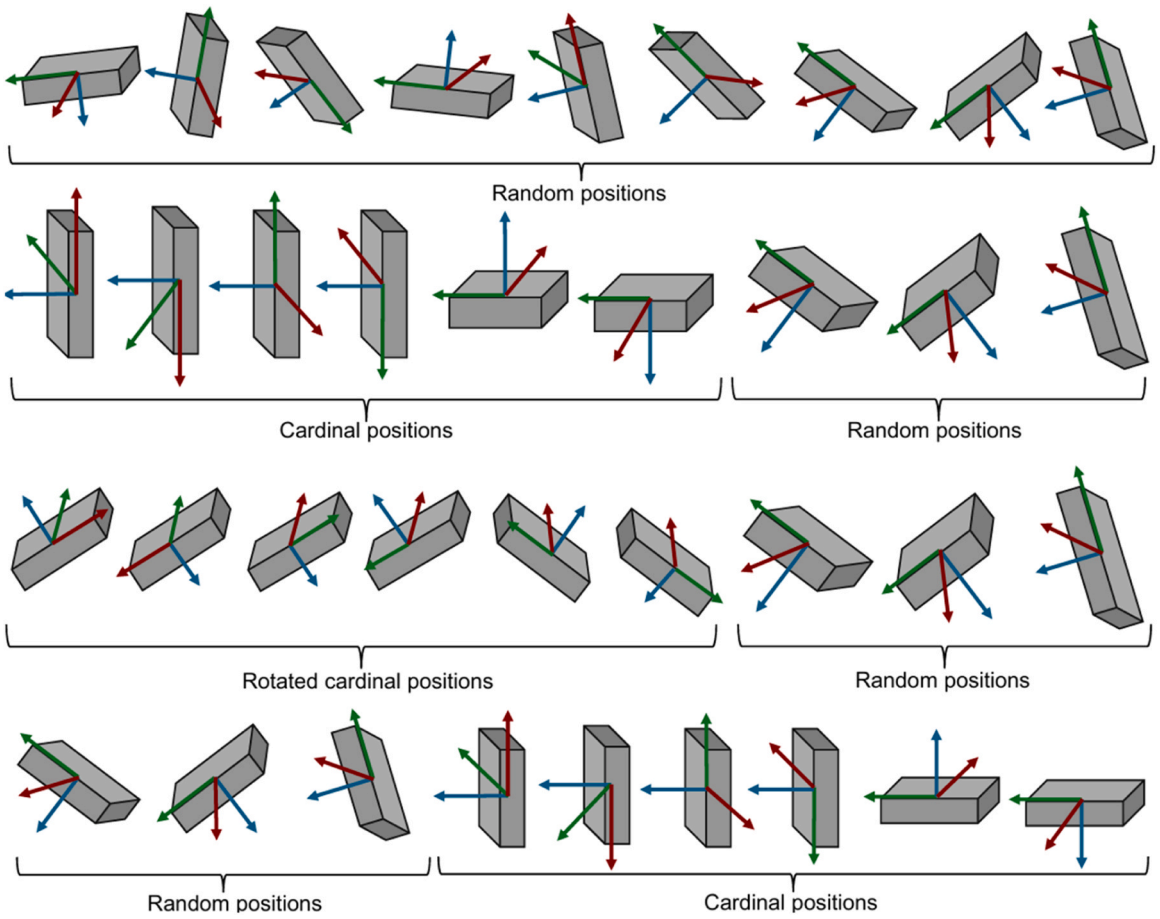


Fig. 2. Four calibration sequences used to study the effect of positions on MPM accuracy.

parameters relative to the axis sensitivities. The rationale behind this was that biases being zeroth order errors, their contribution to the overall measurement error was considered greater than other sources. N is the number of iterations of the Monte Carlo simulation, $k_{ij,true}$ and $k_{ij,est}$ are elements of the true and estimated axis sensitivity matrices respectively, $b_{i,true}$ and $b_{i,est}$ are elements of the true and estimated bias vectors respectively. k and b could take different ranges of values, thus the normalising constants, $k_{ij,norm}$ and $b_{i,norm}$ were introduced to bound each parameter to [0,1]. The normalising bias vector was $b_{norm} = [0.4 \quad 0.4 \quad 0.4]^T$ and normalising axis sensitivity matrix shown in Eq. (15):

$$\mathbf{K}_{norm} = \begin{bmatrix} 0.14 & 0.04 & 0.04 \\ 0.06 & 0.14 & 0.04 \\ 0.06 & 0.06 & 0.14 \end{bmatrix} \tag{15}$$

These capture the range of possible values assuming the linear model in Eq. (1) - Eq. (4) with typical maximum and minimum errors mentioned at the start of 2.1.

The $\overline{CE}$ describes the mean absolute distance of the estimated CPs from their true values. It may be queried why direct evaluation of esti-

mated bias, scale factor, misalignment and nonorthogonality angles was not used as in [17]. The reason is not all methods consider misalignment, not all consider nonorthogonality and some claim to capture both. By evaluating calibration accuracy based on the CPs of the linear model, all methods can be evaluated regardless of their underlying assumptions and is therefore a more model agnostic metric.

For the MPMs (with exception of the closed form methods), it was of interest to observe $\overline{CE}$ based on initialisation of CPs from their true values. Thus, the mean absolute calibration difference ($\overline{MACD}$) was introduced as in Eq. (16):

$$\overline{MACD} = \frac{1}{N}\sum_{n=1}^{N}\left[\frac{1}{9}\sum_{i=1}^{3}\sum_{j=1}^{3}\frac{|k_{ij,true}-k_{ij,init}|}{k_{ij,norm}}+\frac{1}{3}\sum_{k=1}^{3}\frac{|b_{k,true}-b_{k,init}|}{b_{k,norm}}\right] \tag{16}$$

Like $\overline{CE}$, $\overline{MACD}$ features normalisation constants which account for the different ranges of CPs in the accelerometer model. While Eq. (16) was used in the simulations, it could not be used experimentally as the true CPs were unknown. Thus, to observe the influence of parameter initialisation on the MPMs, 1σs in CPs returned by the algorithms for increasing variation in initial parameters from the ideal sensor were studied.

2.3. Experimental setup

Experimental data for the MPM was obtained from the two-axis gimbal in Fig. 3 sampling four LSM6DS3TR-Cs over 30 instances of the procedure, each containing 26 positions as simulated. At each position, the average of 100 samples were taken for consistency with the simulations. As the real platform has dynamics, a half second delay was added after rotating to each position to ensure only the steady state condition was sampled. The total duration of the experimental data was two hours over which the internal sensor temperature drifted less than 0.3° and relative humidity changed by 0.5 %.

In addition to reporting $\overline{CE}$s for SPMs and MPMs, mean squared error (MSE) in bias, SF and nonorthogonality were compared with the CRLB of each static calibration method. The CRLB gives the variance, σ^2_{CRLB}, defining the best achievable precision of an unbiased estimator. Derivation of CRLBs were based on the method in [8], where it was used to benchmark the simulated MPM. MATLAB code for the partial derivatives of measurement models with respect to CPs can be found in the data repository supporting this work.

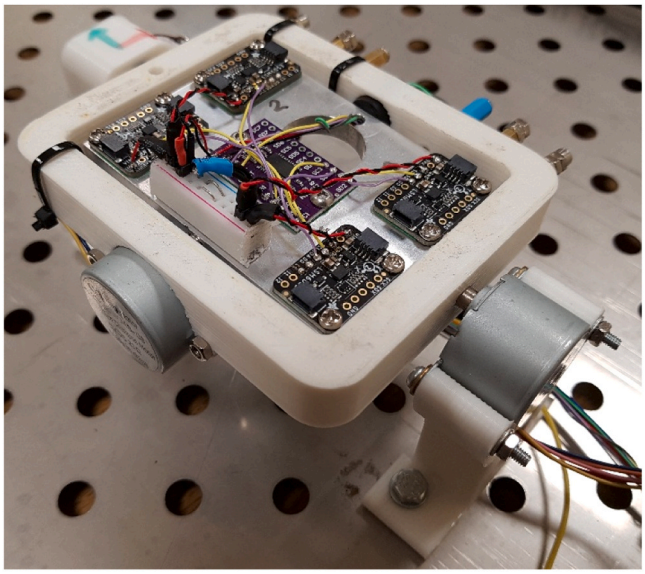


Fig. 3. Two-axis gimbal with IMUs for gathering experimental MPM data.

3. Results

Table 1 shows actual and estimated CPs achieved by the static calibration methods and their corresponding CEs for reference for a simulated calibration.

Table 2 shows the results from 200 iterations of the Monte Carlo simulation for randomised triaxial accelerometers. For each static calibration method, the $\overline{CE}$ and corresponding 1σ are reported, the MAE in estimated angular axis errors are shown as well as the average MSE in calibration for comparison with σ^2_{CRLB} in the final two columns.

Fig. 4 shows the trends in average 1σs in CPs for increasing MACD from the ideal accelerometer. Average 1σs were based on 200 random simulations of the MPM for the four optimisation algorithms.

Table 3 shows the $\overline{CE}$ for the different positions and sequences in the simulated MPM for the case when only nine positions are available.

4. Discussion

The SPM of Jurman et al. which used matrix decompositions to estimate nonorthogonalities as well as misalignment, SFs and biases, gave the lowest $\overline{CE}$, over an order of magnitude lower than all other methods. Referring to the angular MAEs in Table 2, it recovered both nonorthogonality and misalignment angles accurately. Interestingly, average misalignment angles were twice as accuracy as the nonorthogonalities. MSE of the simulated calibration was close to its corresponding CRLB at just $1.3\times\sigma^2_{\text{CRLB}}$ suggesting it is close to the minimum variance unbiased estimator.

The SPM of Ferraris et al. accurately estimated misalignment angles of the sensor with a MAE of 0.011° despite nonorthogonality being present in equal magnitudes in the simulated sensor. This is interesting as Eq. (10) ignores **T** in its calculation of **M** which suggests, if the sensor model described by Eq. (1) – Eq. (5) are representative of the real triaxial accelerometer, misalignment can be accurately estimated without knowledge of nonorthogonalities.

Almost all MPMs achieved the same $\overline{CE}$ of 0.02, marginally larger than the SPM of Ferraris et al. Comparing their $\overline{CE}$s and 1σs, their sim-

Table 1
Actual and estimated CPs with CEs for a random accelerometer model.

Method:	Axis sensitivities:	Biases:	*CE*:
Actual	$\begin{bmatrix}1.0171 & -0.0180 & -0.0080\\ 0.0151 & 1.0061 & -0.0162\\ 0.0102 & 0.0358 & 0.9731\end{bmatrix}$	$\begin{bmatrix}0.0703\\ 0.2399\\ -0.2955\end{bmatrix}$	-
Ferraris et al.	$\begin{bmatrix}1.0169 & -0.0152 & -0.0095\\ 0.0177 & 1.0069 & -0.0359\\ 0.0082 & 0.0160 & 0.9729\end{bmatrix}$	$\begin{bmatrix}0.0725\\ 0.2392\\ -0.2976\end{bmatrix}$	3.5e-2
Jurman et al.	$\begin{bmatrix}1.0168 & -0.0181 & -0.0076\\ 0.0148 & 1.0062 & -0.0159\\ 0.0100 & 0.0359 & 0.9731\end{bmatrix}$	$\begin{bmatrix}0.0725\\ 0.2392\\ -0.2976\end{bmatrix}$	2.6e-3
Tee et al.	$\begin{bmatrix}1.0172 & 0 & 0\\ 0.0150 & 1.0059 & 0\\ 0.0101 & 0.0357 & 0.9725\end{bmatrix}$	$\begin{bmatrix}0.0729\\ 0.2394\\ -0.2960\end{bmatrix}$	3.7e-2
Rohac et al.	$\begin{bmatrix}1.0172 & 0 & 0\\ -0.0027 & 1.064 & 0\\ 0.0019 & 0.0203 & 0.9738\end{bmatrix}$	$\begin{bmatrix}0.0709\\ 0.2394\\ -0.2967\end{bmatrix}$	5.9e-2
Syed et al.	$\begin{bmatrix}1.0171 & 0 & 0\\ -.0027 & 1.0064 & 0\\ 0.0019 & 0.0202 & 0.9738\end{bmatrix}$	$\begin{bmatrix}0.0682\\ 0.2367\\ -0.2928\end{bmatrix}$	6.1e-2
Frosio et al.	$\begin{bmatrix}1.0172 & 0 & 0\\ -0.0027 & 1.0064 & 0\\ 0.0019 & 0.0203 & 0.9738\end{bmatrix}$	$\begin{bmatrix}0.0709\\ 0.2394\\ -0.2967\end{bmatrix}$	5.9e-2
Sipos et al.	$\begin{bmatrix}1.0171 & 0 & 0\\ -0.0027 & 1.0064 & 0\\ 0.0019 & 0.0203 & 0.9738\end{bmatrix}$	$\begin{bmatrix}0.0696\\ 0.2384\\ -0.2935\end{bmatrix}$	6.0e-2
Merayo	$\begin{bmatrix}1.0172 & 0 & 0\\ -0.0028 & 1.0063 & 0\\ 0.0020 & 0.0209 & 0.9740\end{bmatrix}$	$\begin{bmatrix}0.0722\\ 0.2460\\ -0.3018\end{bmatrix}$	6.2e-2
MVEE	$\begin{bmatrix}1.0348 & -0.0029 & 0.0016\\ -0.0029 & 1.0134 & 0.0203\\ 0.0016 & 0.0203 & 0.9491\end{bmatrix}$	$\begin{bmatrix}0.0708\\ 0.2386\\ -0.2966\end{bmatrix}$	8.7e-2

Table 2
$\overline{CE}$s and 1σs, MAEs in axis angular errors and MSE in calibration compared with σ^2_{CRLB} (Monte Carlo simulation N = 200).

Author:	Type:	$\overline{CE}$:	$\sigma_{\overline{CE}}$:	$\overline{MAE}_{\alpha,\beta,\gamma}$ (°):	$\overline{MAE}_{\phi,\theta,\psi}$ (°):	$\overline{MSE}$:	σ^2_{CRLB}:
Ferraris et al.	SPM	1.9e-2	8.7e-3	-	1.1e-2	2.8e-7	2.6e-7
Jurman et al.	SPM	1.2e-3	2.8e-4	2.1e-2	9.2e-3	2.7e-7	2.1e-7
Tee et al.	SPM	1.4e-2	6.1e-3	0.26	-	1.2e-5	2.7e-7
Rohac et al.	MPM	2.0e-2	8.5e-3	7.4e-3	-	1.9e-7	6.1e-8
Syed et al.	MPM	2.0e-2	8.5e-3	7.5e-3	-	2.3e-6	6.1e-8
Frosio et al.	MPM	2.0e-2	8.5e-3	9.6e-3	-	2.0e-7	6.1e-8
Sipos et al.	MPM	2.0e-2	8.6e-3	7.4e-3	-	2.2e-6	6.1e-8
Merayo	MPM	2.0e-2	8.5e-3	9.4e-3	-	1.3e-6	6.1e-8
MVEE	MPM	3.7e-2	1.2e-2	1.3e-2	0.37	1.3e-4	6.1e-8

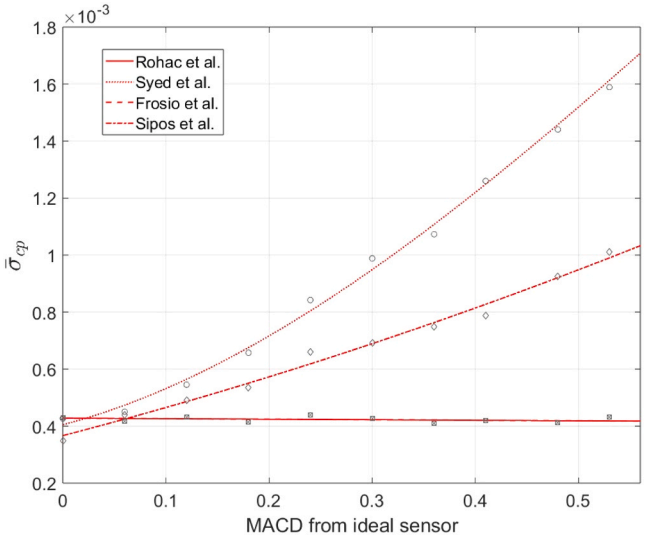


Fig. 4. Average 1σs in CPs obtained by iterative MPMs with increasing distance in initialisation conditions from the ideal sensor (Monte Carlo simulation N = 200).

Table 3
$\overline{CE}$s and 1σs for four MPM sequences (Average of all algorithms, Monte Carlo simulation N = 200).

Sequence of nine positions:	$\overline{CE}$:	$\sigma_{\overline{CE}}$:
Random	0.38	0.27
Cardinal + three rdn.	0.034	0.018
Rotated cardinal + three rdn.	0.27	0.81
Three rdn. + cardinal	0.032	0.017

ilarity reflects the inability of the former to capture misalignments and the latter, nonorthogonalities, when the accelerometer was modelled with both sources of error. In Table 1, off-diagonal terms in the axis sensitivity matrices for Ferraris et al. and the MPMs were inconsistent with the actual values.

Despite assuming the same model, the $\overline{CE}$ for Tee et al. was 30 % lower than that of the MPMs. This was because the former compensated for the combined effect of nonorthogonality and misalignment. Comparing the $\overline{CE}$ with that of Ferraris et al. where the misalignment angles were estimated instead of nonorthogonalities, there was a 30 % reduction for Tee et al. This shows the ability of the method to compensate for the combined angular errors in the lower triangular part of the axis sensitivity matrix. However, referring to $\overline{MAE}_{\alpha,\beta,\gamma}$ for Tee et al. in Table 2, estimated nonorthogonalities were not representative of the actual values inserted into the accelerometer model. The average error of 0.26° corresponds to being no better than random guessing within the specified bounds. The lower $\overline{CE}$ of Tee et al. therefore shows it accurately estimated off-diagonal parameters of the axis sensitivity matrix when there were both misalignment and nonorthogonality errors but the actual nonorthogonality angles could not be recovered.

MPMs gave $\overline{CE}$s higher than Tee et al. because, for the simulated conditions, they could not detect and compensate for the combination of axis misalignments and nonorthogonalities which influence CPs in the lower triangular part of the axis sensitivity matrix. The MPM is unable to detect axes misalignment because the misalignment matrix has unit norm and thus has no effect on the magnitude of the measurements. Indeed, for MVEE in Table 2, MAE in misalignment angles was slightly worse than random guessing at 0.37°. While this gave MPMs a higher $\overline{CE}$ than Tee et al., it had a benefit. MAEs in nonorthogonality angles were accurately estimated by all MPMs with lowest error achieved by the methods of Rohac et al. and Sipos et al. Thus, the MPM can estimate nonorthogonality angles between axes, even if those axes are misaligned relative to the calibration platform.

$\overline{CE}$s for MPMs in Table 2 were all 0.02 except for MVEE which was almost twice as high. Similarity among the MPMs is unsurprising given the Q-N, L-M and G-N algorithms derive from Newton's method. Rohac et al. used the Q-N method which approximates the Hessian matrix instead of computing it directly. While this can be useful when the Hessian is poorly conditioned, this appears not to be the case in the simulated MPM. Thus, the approximation offered little advantage over the G-N algorithm. The same applies to the L-M algorithm in Sipos et al. which adds damping to Newton's method in case of poorly conditioned Hessians. This makes convergence slower and for each instance of the simulation, the L-M algorithm stopped due to exceeding the maximum number of iterations. In comparison, the G-N method converged to a solution within 10–20. Regarding precision, the Q-N of Rohac et al. came the closest to the CRLB (MSE about $3\times\sigma^2_{\text{CRLB}}$) agreeing with the values reported in [8]. The better precision of the Q-N method could be due to its mentioned Hessian approximation. MVEE was the worst performing MPM corroborating the findings in [17]. This may have been due to the implicit assumption of a symmetric axis sensitivity matrix which was not captured in the sensor model. Interestingly, the z-axis scale factor for MVEE in Table 1 was particularly erroneous compared with x and y. The variance of the CRLB in Table 2 was lower for the MPMs than the SPMs because it sampled 26 positions instead of six.

Fig. 5 and Fig. 6 show histograms of accelerometer biases, scale factors and nonorthogonality angles estimated by the MPM of Rohac et al. based on experimental data from four LSM6DS3TR-Cs. Their distributions are compared against 1σs in parameters from the simulated calibration and the CRLB. In Fig. 5(a)-(d), biases had 1σs almost twice than simulated and about $3\times\sigma^2_{\text{CRLB}}$. Precision in nonorthogonality angles was comparatively better with 1σs just 20 % larger than simulated and $2.7\times\sigma^2_{\text{CRLB}}$ as shown in Fig. 6. Fig. 5(e)-(h) show experimental precision in SFs matched the simulations better, having 1σs just 16 % larger than simulated and $1.8\times\sigma^2_{\text{CRLB}}$. While experimental data was gathered in a controlled environment and the sensor allowed two hours warm up time, additional heating transferred from the gimbal's motors may have caused the 0.3°C increase in the chip's internal temperature resulting in larger 1σs than simulated.

Table 3 shows the $\overline{CE}$ and 1σ for four different MPM sequences. It was assumed the minimum possible (nine) positions were available hence $\overline{CE}$s were higher than in Table 2 where 26 positions were used. The results show how cardinal positions gave a $\overline{CE}$ about ten times lower

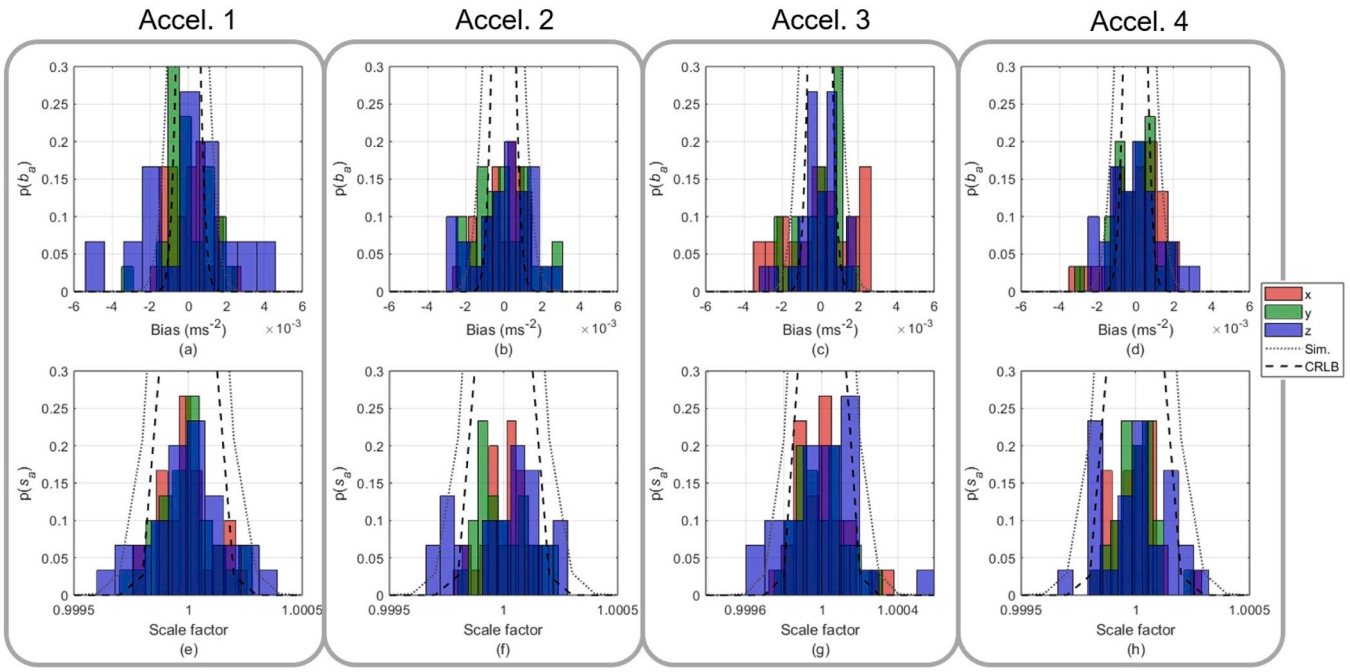


Fig. 5. Histograms of mean subtracted experimental biases (a-d) and unit centred SFs (e-h) for triaxial accelerometers 1–4 respectively. 1σs of simulations and CRLB plotted for comparison.

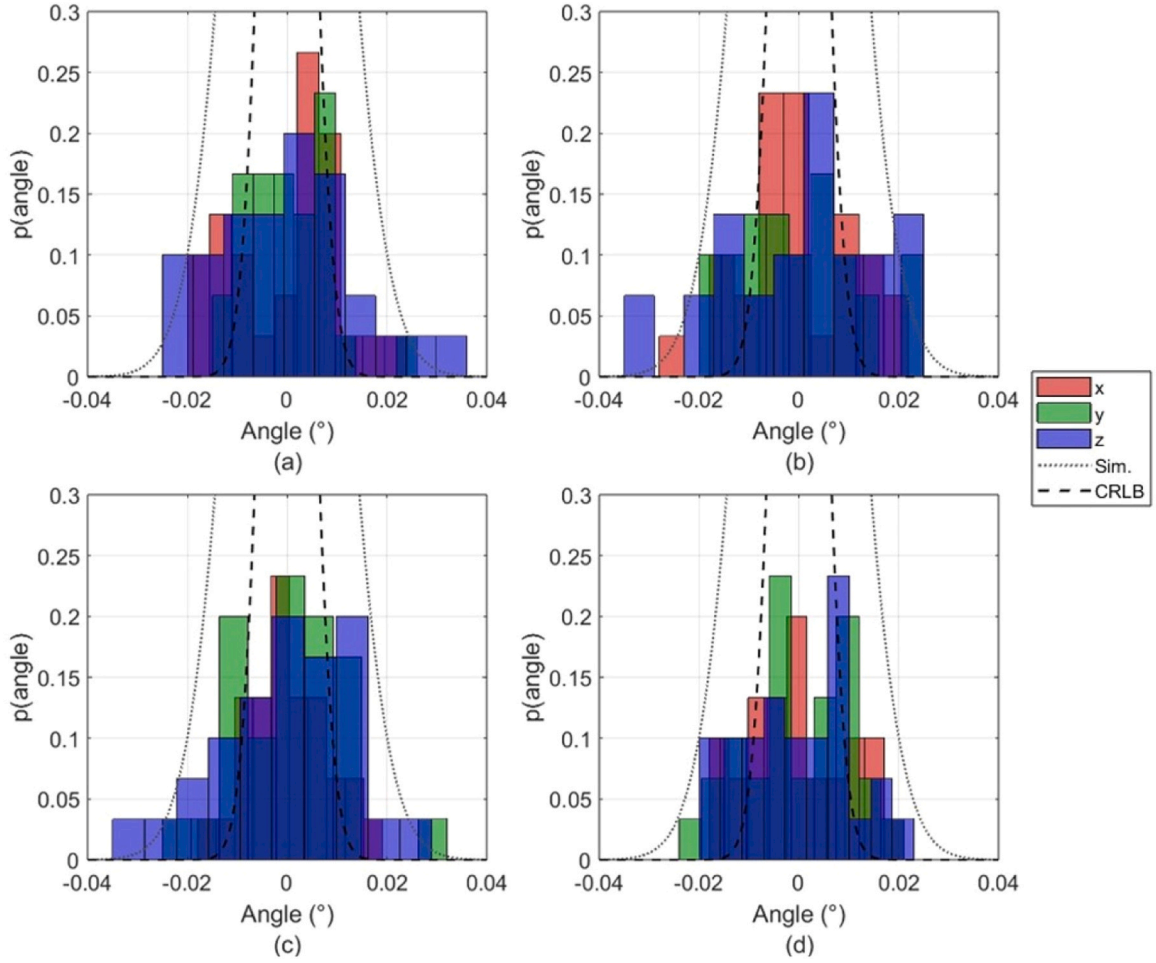


Fig. 6. (a)-(d) Histograms of mean subtracted experimental nonorthogonalities for accelerometers 1–4 respectively. 1σs of simulations and CRLB plotted for comparison.

than random positions and the rotated cardinal case. For the permuted cardinal cases, there was no great difference in $\overline{CE}$ suggesting the order of sampling in the MPM is unimportant.

Plots of 1σs in estimated CPs with MACD from the ideal sensor in Fig. 4 show how some of the simulated MPMs (Rohac et al. and Frosio et al.) were unaffected by parameter initialisation. Of the MPMs tested, the most affected by initialisation was the least squared adjustment method of Syed et al., followed by the L-M algorithm used in Sipos et al. The experimental results in Fig. 7 agree with the simulation, showing the same vulnerability in two of the MPMs. Use of the methods of Rohac et al. and Frosio et al. are therefore recommended for more precise calibration.

5. Conclusion

Both simulation and experimental results confirmed the MPMs of Rohac et al. and Frosio et al. were unaffected by CP initialisation when typical values from the bounds in the datasheet were used. This was not the case for the methods of Syed et al. and Sipos et al. Of the MPMs, Monte Carlo simulation showed the best performing algorithms were those of Rohac et al. and Frosio et al., the former achieving the closest MSE to the CLRB. Experimental results showed how the MPM of Rohac et al. was close to the CRLB in terms of scale factor and nonorthogonality angles suggesting it is close to the minimum variance unbiased estimator. For the MPMs, Monte Carlo simulation showed sampling the cardinal positions first gave the lowest $\overline{CE}$ with their order being unimportant.

The results showed the SPM of Jurman et al. gave the lowest $\overline{CE}$ of all the calibration methods and recovered all angular errors. While the SPM of Tee et al. did not include misalignment in its model, it had the second lowest $\overline{CE}$ by compensating the combined effects of nonorthogonality and misalignment but the physical nonorthogonality angles were not recoverable.

Though the SPM of Jurman et al. gave the lowest $\overline{CE}$, it assumed Eq. (1)-Eq. (4) were an accurate model of the real MEMS accelerometer which was also the basis of the simulations. It is not known whether it is best in terms of accurately capturing the behaviour of open loop proof mass MEMS accelerometers. Indeed, in Frosio et al., a symmetric axis sensitivity matrix was used explaining it better captured cross-coupling effects between axes. Though the SPM of Jurman et al. gave the lowest $\overline{CE}$, caution should be taken in the interpretation of the estimated misalignment and nonorthogonality angles as they may not be representative of the physical system. As mentioned in Hiller et al., to make nonorthogonality angles unique, one axis must be chosen as the reference, giving **T** triangular structure. This may not be representative of the real system however so the results in Table 2 should be approached with caution.

Future work may address the following: Experimental validation of different measurement models to find which is more representative of the actual MEMS accelerometer, assess the accuracy of minimisation of magnitude of measurements relative to gravity as representative of accurate calibration, assess the effect of different choices of 'fixed axis' in the nonorthogonality assumption on calibration accuracy and investigate the reason for the sensitivity of parameter initialisation seen in the MPMs of Sipos et al. and Syed et al.

CRediT authorship contribution statement

Simon Trythall: Resources. **Robert Cooper:** Resources. **Stuart Kitching:** Resources. **Economou John Theodoros:** Writing – review & editing, Visualization, Supervision, Project administration. **Dariusz Maton:** Writing – original draft, Validation, Software, Methodology, Investigation, Formal analysis, Data curation, Conceptualization. **Khan Irfan Ullah:** Writing – review & editing, Supervision. **David Galvão Wall:** Writing – review & editing, Supervision.

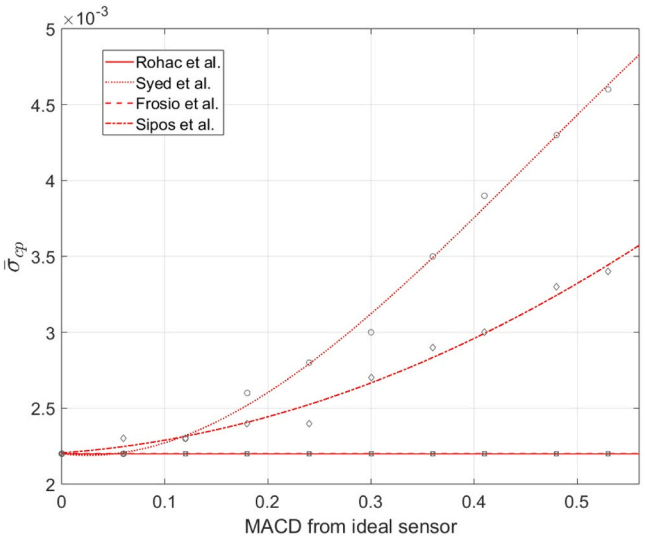


Fig. 7. Average 1σs in CPs obtained by iterative MPMs with increasing distance in initialisation conditions from the ideal sensor.

Funding

This work was supported by the EPSRC iCASE grant reference EP/S513623/1, BAE Systems and Cranfield University.

Declaration of Competing Interest

The authors declare the following financial interests/personal relationships which may be considered as potential competing interests: Dariusz Maton reports financial support was provided by Engineering and Physical Sciences Research Council. Dariusz Maton reports financial support was provided by BAE Systems. Dariusz Maton reports financial support was provided by Cranfield University. If there are other authors, they declare that they have no known competing financial interests or personal relationships that could have appeared to influence the work reported in this paper.

Data availability

Data and algorithms relating to the work are available on the Cranfield University research data repository (CORD) at: https://doi.org/10.57996/cran.ceres-2776.

References

[1] A. Noureldin, T.B. Karamat, J. Georgy, Satellite-based Positioning and their Integration. Fundamentals of Inertial Navigation, Springer Berlin Heidelberg, Berlin, Heidelberg, 2013, https://doi.org/10.1007/978-3-642-30466-8.
[2] R. Raya, J.O. Roa, E. Rocon, R. Ceres, J.L. Pons, Wearable inertial mouse for children with physical and cognitive impairments, Sens Actuators A Phys. 162 (2010) 248–259, https://doi.org/10.1016/j.sna.2010.04.019.
[3] S.K. Hong, Fuzzy logic based closed-loop strapdown attitude system for unmanned aerial vehicle (UAV), Sens Actuators A Phys. 107 (2003) 109–118, https://doi.org/10.1016/S0924-4247(03)00353-4.
[4] M.L. Hoang, A. Pietrosanto, Yaw/Heading optimization by drift elimination on MEMS gyroscope, Sens Actuators A Phys. 325 (2021) 112691, https://doi.org/10.1016/j.sna.2021.112691.
[5] V. Kempe, Inertial MEMS: Principles and Practice, Cambridge University Press, Cambridge, 2011 https://doi.org/DOI: 10.1017/CBO9780511933899.
[6] F. Gulmammadov, Analysis, modeling and compensation of bias drift in MEMS inertial sensors, in: 4th International Conference on Recent Advances in Space Technologies, 2009, IEEE, Istanbul, 2009, pp. 591–596, https://doi.org/10.1109/RAST.2009.5158260.
[7] K.R. Britting, Inertial Navigation Systems Analysis, John Wiley & Sons, Inc, 1971.
[8] I. Skog, P. Händel, Calibration of a MEMS Inertial Measurement Unit, in: XVII IMEKO World Congress, Rio de Janeiro, 2006.
[9] T. Hiller, L. Blocher, M. Vujadinovic, Z. Pentek, A. Buhmann, H. Roth, Analysis and Compensation of Cross-Axis Sensitivity in Low-Cost MEMS Inertial Sensors, in:

INERTIAL 2021 - 8th IEEE International Symposium on Inertial Sensors and Systems, Proceedings, Institute of Electrical and Electronics Engineers Inc., 2021. https://doi.org/10.1109/INERTIAL51137.2021.9430454.
[10] F. Ferraris, U. Grimaldi, M. Parvis, Procedure for effortless in-field calibration of three-axis rate gyros and accelerometers, Sens. Mater. 7 (1995) 311–330, https://doi.org/10.1016/0924-4247(94)80031-6.
[11] Z.F. Syed, P. Aggarwal, C. Goodall, X. Niu, N. El-Sheimy, A new multi-position calibration method for MEMS inertial navigation systems, Meas. Sci. Technol. 18 (2007) 1897–1907, https://doi.org/10.1088/0957-0233/18/7/016.
[12] M. Šipoš, P. Pačes, J. Roháč, P. Nováček, Analyses of triaxial accelerometer calibration algorithms, IEEE Sens J. 12 (2012) 1157–1165, https://doi.org/10.1109/JSEN.2011.2167319.
[13] K.S. Tee, M. Awad, A. Dehghani, D. Moser, S. Zahedi, Triaxial Accelerometer Static Calibration, in: S.I. Ao, L. Gelman, D.W.L. Hukins, A. Hunter, A.M. Korsunsky (Eds.), Proceedings of the World Congress on Engineering 2011, Newswood Ltd, London, 2011, pp. 2164–2167.
[14] D. Jurman, M. Jankovec, R. Kamnik, M. Topič, Calibration and data fusion solution for the miniature attitude and heading reference system, Sens Actuators A Phys. 138 (2007) 411–420, https://doi.org/10.1016/j.sna.2007.05.008.
[15] I. Frosio, F. Pedersini, N.A. Borghese, Autocalibration of MEMS accelerometers, IEEE Trans. Instrum. Meas. 58 (2009) 2034–2041, https://doi.org/10.1109/TIM.2008.2006137.
[16] J.C. Lötters, J. Schipper, P.H. Veltink, W. Olthuis, P. Bergveld, Procedure for in-use calibration of triaxial accelerometers in medical applications, Sens Actuators A Phys. 68 (1998) 221–228, https://doi.org/10.1016/S0924-4247(98)00049-1.
[17] S. Bonnet, C. Bassompierre, C. Godin, S. Lesecq, A. Barraud, Calibration methods for inertial and magnetic sensors, Sens. Actuators A Phys. 156 (2009) 302–311, https://doi.org/10.1016/j.sna.2009.10.008.
[18] J. Rohac, M. Sipos, J. Simanek, Calibration of low-cost triaxial inertial sensors, IEEE Instrum. Meas. Mag. 18 (2015) 32–38, https://doi.org/10.1109/MIM.2015.7335836.
[19] I. Frosio, S. Stuani, N.A. Borghese, Autocalibration of MEMS Accelerometer, in: IEEE Instrumentation and Measurement Technology Conference Proceedings, 2006, IEEE, 2006, pp. 519–523, https://doi.org/10.1109/IMTC.2006.328554.
[20] E.H. Shin, N. El-Sheimy, A new calibration method for strapdown inertial navigation systems, Z. Vermess. 127 (2002) 1–10.
[21] L. Ye, A. Argha, B.G. Celler, H.T. Nguyen, S.W. Su, Online auto-calibration of triaxial accelerometer with time-variant model structures, Sens Actuators A Phys. 266 (2017) 294–307, https://doi.org/10.1016/j.sna.2017.08.049.
[22] M. Glueck, D. Oshinubi, P. Schopp, Y. Manoli, Real-time autocalibration of MEMS accelerometers, IEEE Trans. Instrum. Meas. 63 (2014) 96–105, https://doi.org/10.1109/TIM.2013.2275240.
[23] S. Khankalantary, S. Ranjbaran, S. Ebadollahi, Simplification of calibration of low-cost MEMS accelerometer and its temperature compensation without accurate laboratory equipment, Meas. Sci. Technol. 32 (2021), https://doi.org/10.1088/1361-6501/abd0bf.
[24] J. Včelák, P. Ripka, J. Kubík, A. Platil, P. Kaňpar, AMR navigation systems and methods of their calibration, Sens Actuators A Phys. 123124 (2005) 122–128, https://doi.org/10.1016/j.sna.2005.02.040.
[25] J.M.G. Merayo, P. Brauer, F. Primdahl, J.R. Petersen, O.V. Nielsen, Scalar calibration of vector magnetometers, Meas. Sci. Technol. 11 (2000) 120–132, https://doi.org/10.1088/0957-0233/11/2/304.
[26] N. Moshtagh, Minimum Volume Enclosing Ellipsoid, MATLAB File Exchange (2007). https://uk.mathworks.com/matlabcentral/fileexchange/9542-minimum-volume-enclosing-ellipsoid (accessed June 4, 2025).
[27] D.E. Wells, E.J. Krakiwsky, A Synthesis of Recent Advances in the Method of Least Squares, 1971. https://gge.ext.unb.ca/Pubs/LN42.pdf (accessed October 22, 2024).
[28] E.-H. Shin, UCGE Reports Accuracy Improvement of Low Cost INS/GPS for Land Applications, Calgary, 2001. ⟨https://www.ucalgary.ca/engo_webdocs/NES/01.20156.EHShin.pdf⟩ (accessed November 4, 2024).
[29] B. Kumar, MEMS Accelerometer Calibration using Gauss Newton Method, MATLAB Central File Exchange (2011). ⟨https://uk.mathworks.com/matlabcentral/fileexchange/33252-mems-accelerometer-calibration-using-gauss-newton-method⟩ (accessed October 10, 2024).

Dariusz Maton – Teaching Fellow at Cranfield University. His undergraduate studies were in Aerospace Engineering at The University of Manchester. His current area of work centres on low-cost inertial sensors.

Prof. John Economou - Professor Economou is a Professor of Defence Robotics and Autonomous Systems. After his service as the Deputy Head Centre for Defence Engineering at Cranfield Defence and Security and Head of the Vehicles and Mechatronics Group, he is currently the Deputy Director of Consultancy for Defence and Security PVC office.

Dr. David Gavlão Wall - David is Head of the Air Platforms and Weapons Group. He is also the Course Director for the university's Guided Weapon Systems MSc Course at Shrivenham.

Dr. Irfan Ullah Khan - Dr. Irfan Khan is a Lecturer in Mechatronics within the Autonomy and Mechatronics Group at the Centre for Defence Engineering and Physical Sciences, based at Cranfield Defence and Security, Shrivenham.

Mr. Robert Cooper - has a City and Guilds certificate in Motor Vehicle Craft Studies and a HND in Automotive Engineering. He joined the British Army in 1992. Mr. Cooper joined Cranfield University in 2017 and is currently a Laboratory Manager.

Mr. Simon Trythall - graduated from the University of Birmingham and has worked on magnetic, optical, and inertial helmet tracking systems installed on several fixed and rotary wing aircraft.

Mr. Sturart Kitching - Technology Manager at BAE Systems.



https://dspace.org/

Experimental-based Cramér-Rao lower bound estimation of triaxial accelerometer calibration methods using Monte Carlo simulation

Maton, Dariusz; Economou, John T.; Galvão Wall, David; Khan, Irfan; Cooper, Robert ...

2026-01-01
Elsevier
https://doi.org/10.1016/j.sna.2025.117300
Maton D, Economou JT, Wall DG et al., (2026) Experimental-based Cramér-Rao lower bound estimation of triaxial accelerometer calibration methods using Monte Carlo simulation. Sensors and Actuators A: Physical, Volume 397, January 2026, Article number 117300

Downloaded from a DSpace repository. https://dspace.org/